

Anchorless Cooperative Tracking Using Multipath Channel Information

Josef Kulmer, *Student Member, IEEE*, Erik Leitinger, *Member, IEEE*, Stefan Grebien, *Student Member, IEEE*, and Klaus Witrissal, *Member, IEEE*

Abstract—Highly accurate location information is a key facilitator to stimulate future services for the commercial and public sectors. Positioning and tracking of absolute positions of wireless nodes usually requires information provided from technical infrastructure, e.g. satellites or fixed anchor nodes, whose maintenance is costly and whose limited operating coverage narrows the positioning service. In this paper we present an algorithm aiming at tracking of absolute positions without using information from fixed anchors, odometers or inertial measurement units. We perform radio channel measurements in order to exploit position-related information contained in multipath components (MPCs). Tracking of the absolute node positions is enabled by estimation of MPC parameters followed by association of these parameters to a floorplan. To account for uncertainties in the floorplan and for propagation effects like diffraction and penetration, we recursively update the provided floorplan using the measured MPC parameters. We demonstrate the ability to localize two agent nodes without the employment of further infrastructure, using data from ultra-wideband channel measurements. Further, we show the potential performance gain if also one fixed anchor is available and we validate the algorithm for a range of different signal bandwidths and number of nodes.

I. INTRODUCTION

Many applications in wireless radio networks demand knowledge of the nodes' absolute positions. Two types of nodes are considered, namely mobile agents and fixed anchors with unknown and known positions, respectively. The agents intend to track their positions using measurements of position-related signal parameters obtained from radio transmissions to the anchors [1]. To ensure an accurate positioning, highly effective measurements are necessary. In practice, the measurements are often disturbed, especially in harsh radio propagation environments e.g. in urban areas or indoors. Reliable measurements are hindered due to the limited coverage of global navigation satellite systems, radio-propagation effects e.g. multipath propagation and non-line-of-sight (NLOS) conditions, or interference by other agents. Several attempts to encounter adverse radio propagation effects have been proposed, e.g. identification and mitigation of NLOS conditions [2]–[4], data fusion of multiple information sources [5] or providing remedies against the errors induced by the multipath propagation [6].

J. Kulmer, S. Grebien and K. Witrissal are with the Laboratory of Signal Processing and Speech Communication, Graz University of Technology, Graz, Austria, (e-mail: {kulmer, stefan.grebien, witrissal}@tugraz.at). E. Leitinger is with the Department of Electrical and Information Technology, Lund University, Lund, Sweden (e-mail: erik.leitinger@eit.lth.se).

A promising idea to deal with multipath propagation is utilization rather than mitigation. Multipath components (MPCs) originate at objects, e.g. planar surfaces and walls. Assuming the objects' locations are known a-priori or learned from previous measurements then the agents can take advantage of the position-related information contained in the MPCs [7]–[18].

The methods presented in [9]–[11] associate MPCs to the surrounding geometry yielding the possibility to track the agents' absolute positions with a single anchor only. To push the limits of accuracy and robustness, the methods in [12]–[16] introduce cooperation among the agents too. In [12] the performance gain was shown in terms of position error for a varying number of cooperating agents and a single anchor. In [13] the mathematical model is relaxed to a convex optimization problem. The gained performance is demonstrated for two agents and three anchors.

The availability of only a small number of anchors and cooperating agents results in a limited number of measurements which can be used for positioning. To encounter ambiguities and inaccuracies, the methods in [14]–[16] assume the employment of *self* measurements, where each agent is equipped with a transmitting and a receiving antenna located next to each other. Measuring the channel impulse response between these antennas enables the estimation of MPCs whose parameters depend only on one agent's position (and antenna properties) as well as the surrounding environment. These measurements therefore serve as an attractive additional information source for the task of positioning.

In this work we present an anchor-free, centralized, cooperative tracking algorithm. It takes advantage of position-related information contained in the measured channel impulse responses. We consider *relative* measurements between neighboring agents and *self* measurements where the agents act simultaneously as transmitters and receivers. Such a setup applies for example to applications in a Car-To-X scenario, emergency service personnel entering a building, and (automated) vehicles in a production facility. The proposed algorithm estimates parameters of deterministic MPCs and associates the estimated delays to expected ones. To calculate the expected delays, we consider planar surfaces (e.g. walls) in an indoor environment described by a provided floorplan. To account for inaccuracies in the floorplan, as well as for effects like penetration and diffraction of the electromagnetic waves, the associated MPC delays are used to simultaneously adapt the floorplan while tracking the agents' positions. The proposed method aims at refining the (possibly inaccurate) floorplan

rather than discovering additional features (as proposed in SLAM [19]). We assume a static environment.

The key contributions of this paper are:

- We formulate the relationship between the agent positions, the environment model and the measured MPC delays. It is assumed that agents are synchronized with each other.
- We present an anchor-free, centralized, cooperative algorithm using data association of MPC delays and formulate an extended Kalman filter (EKF) for simultaneous tracking of the agents' positions and the floorplan.
- We demonstrate the ability of the algorithm to track agents without information obtained from fixed anchors or an inertial measurement unit.
- We recursively update the environment model to remedy uncertainties in the provided floorplan.
- We show the performance in adverse scenarios considering a varying number of agents and channel bandwidths.

The paper is organized as follows: Section II provides an overview of the problem and introduces the signal and geometry models. Section III describes the implementation of the cooperative algorithm. Section IV presents an evaluation and discussion using a static environment and Sec. V wraps up the paper with a conclusion. We note that this work extends our conference publication [16], in what follows. We introduce a geometry model for relating MPC delays to agent positions as well as environment features. We verify the performance gain for a varying number of agents, consider the influence of the channel bandwidth and the impact of obtaining range information from a fixed anchor.

II. PROBLEM FORMULATION

Consider a synchronized network of agents $m \in \mathcal{M} = \{1, \dots, M\}$ located in an indoor-environment as shown in Fig. 1. The agents aim at estimating their positions¹ $\{\mathbf{p}^{(m)}\}$ using radio signals affected by multipath propagation. The multipath propagation originates from the interaction of the transmitted unit-energy signal $s(t)$ with its surrounding environment, e.g. reflections at flat surfaces like wall segments. The time delays of the reflections convey information about the surrounding environment and can be exploited for localizing the agents.

We use UWB signals motivated by their superior time resolution which enables a temporal separation of the multipath components in indoor environments. We employ *self* and *relative* channel measurements conducted by the agents. The self measurement is individually performed by each agent m by emitting the signal $s(t)$ and receiving the corresponding superposition of reflections originating at the surrounding environment. The relative measurements are performed by two cooperating agents m and m' , yielding a received signal composed of the sum of the line-of-sight (LOS) and multipath components. The delays of the components depend on both

¹Similar to [7], [13], [17], [20]–[22] we model the agent's positions and the surrounding environment in two dimensions. The restriction is reasonable since most positioning applications have knowledge about the agent's height and the extension to three dimensions is straight-forward.

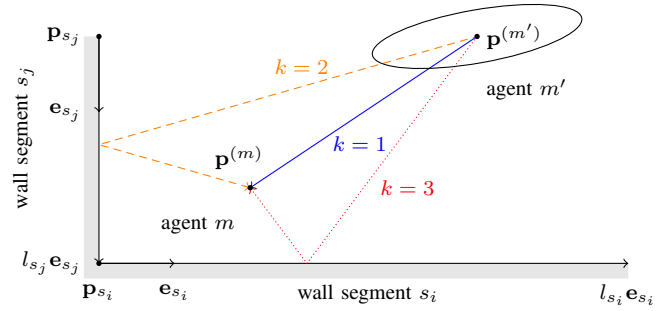


Fig. 1. Illustration of cooperative localization utilizing multipath propagation. The receiving agent m facilitates the MPCs $k \in \mathcal{K}^{(m',m)} = \{1, 2, 3\}$ for localization. The transmitting agent m' is uncertain about its position, represented by the ellipse. The higher position uncertainty of m' in direction of MPC $k = 2$ compared to $k = 3$ needs to be accounted by agent m .

agents' positions, indicating that the position accuracy of cooperating agents is related as well [7], [23]–[25].

A. Signal Model

We model the baseband-equivalent received signal $r^{(m',m)}(t)$ of agent m for the emitted signal $s(t)$ of agent m' according to [7], [26]

$$r^{(m',m)}(t) = \sum_{k \in \mathcal{K}^{(m',m)}} \alpha_k^{(m',m)} s(t - \tau_k^{(m',m)}) + (s * \nu^{(m',m)})(t) + w(t). \quad (1)$$

The first term on the right-hand-side denotes the deterministic MPCs which can be related to an environment model. The set $\mathcal{K}^{(m',m)}$ contains the modeled MPCs at agents' positions $\mathbf{p}^{(m)}$ and $\mathbf{p}^{(m')}$. Each deterministic MPC $k \in \mathcal{K}^{(m',m)}$ is characterized by its amplitude $\alpha_k^{(m',m)}$ and delay $\tau_k^{(m',m)}$. The relation between MPC delays, agent positions and the surrounding environment will be further discussed in Sec. II-B.

The second term of (1) covers all *residual* components which are not modeled by the environment model as well as scattering at small objects or rough surfaces. It is defined as the convolution of $s(t)$ with diffuse multipath (DM) $\nu^{(m',m)}(t)$. We model DM as a zero-mean Gaussian random process which is non-stationary in the delay domain τ , defined by the auto-correlation function $\mathbb{E}\{\nu^{(m',m)}(\tau)[\nu^{(m',m)}(u)]^*\} = S_\nu^{(m',m)}(\tau)\delta(\tau - u)$ where $S_\nu^{(m',m)}(\tau)$ denotes the power delay profile (PDP) of DM. The PDP is quasi-stationary in the spatial domain. At the large scale, it is a function of the positions of transmitter and receiver, determined by the surrounding environment [27].

The last term denotes additive white Gaussian noise with a double-sided power spectral density of $N_0/2$. The signal model in (1) is applied for the relative measurements ($m \neq m'$) as well as for the self measurements by setting $m = m'$.

B. Geometry model

The agents are capable of estimating the MPC delays from the received signal. To link the estimated delays to the environment, we employ a geometry model as illustrated in Fig. 1. Agent m receives the emitted pulse of agent m' as a sum of the LOS component and reflections at wall segments

s_i and s_j .

We consider reflections originating at planar surfaces, e.g. walls, doors, and windows, in the following denoted as *wall segments*. Each wall segment $s \in \mathcal{S} = \{1, \dots, S\}$ is described by its location $\mathbf{p}_s \in \mathbb{R}^2$ (an end point of the wall segment) and orientation $l_s \mathbf{e}_s$ with l_s as length and the unit-vector $\mathbf{e}_s \in \mathbb{R}^2$ as the direction of the wall segment as illustrated in Fig. 1.

The wall segments reflecting the deterministic MPC k are denoted by $\mathbf{s}_k^{(m',m)}$, consisting of the indices of the wall segments $\mathbf{s}_k^{(m',m)} = [s_1, \dots, s_I]$, with I as number of reflecting segments, in the following referenced as *reflection order*.

Given the geometry model, the delays of both the LOS and the reflections can be denoted as a function of the interacting agents $\mathbf{p}^{(m)}$ and $\mathbf{p}^{(m')}$, and the bounced wall segments, denoted as

$$\tau_k^{(m',m)} = \frac{1}{c} d(\mathbf{p}^{(m')}, \mathbf{p}^{(m)}, \mathbf{s}_k^{(m',m)}) \quad (2)$$

where c is the speed of light (see Appendix A for the derivation).

As we assume a reciprocal channel between m' and m , the MPC delays are equal whether m' acts as the receiver or transmitter, i.e. $\tau_k^{(m',m)} = \tau_k^{(m,m')}$ (see Appendix B). We consider a two-dimensional environment model. Reflections which are not contained in the geometry model (e.g. reflections by floor or ceiling, or at furniture) are treated as DM in (1).

III. PROPOSED ALGORITHM

The proposed algorithm tracks the agent's positions as well as the locations of the wall segments using an EKF [19]. We describe the state dynamics by the joint state vector \mathbf{x}_n with discrete time step n by employing a state-space and a measurement model

$$\text{state-space model: } \mathbf{x}_n = f(\mathbf{x}_{n-1}) + \mathbf{n}_{a,n} \quad (3)$$

$$\text{measurement model: } \mathbf{z}_n = h(\mathbf{x}_n) + \mathbf{n}_n \quad (4)$$

where $\mathbf{n}_{a,n}$ and \mathbf{n}_n are the process noise and measurement noise, respectively. The EKF² estimates the agents' positions $\{\mathbf{p}_n^{(m)} : m \in \mathcal{M}\}$ and the locations of the wall segments $\{\mathbf{p}_s : s \in \mathcal{S}\}$ using the estimated MPC delays $\{\hat{d}_{k,n}^{(m',m)} = c\hat{\tau}_{k,n}^{(m',m)} : m, m' \in \mathcal{M}\}$ (scaled by c), as measurement input of the filter. Note, the joint state vector \mathbf{x}_n is introduced in Sec. III-D and time step n has been added to position vectors and MPC delays.

The algorithm is formulated by a prediction and an update step. At the prediction step the movement of the agents is modeled by a constant-velocity motion model (Sec. III-A) using (3). The update step predicts the multipath propagation employing the geometry model of Section II-B and updates the agent positions and the wall segment locations (Sec. III-D) using (4).

²The choice of the EKF is reasoned due to the weak non-linearity of the measurement model in the vicinity of the linearization point.

A. State-space model of agents

We use a constant-velocity motion model to track the agents' positions. The state vector of a single agent m is characterized by its position $\mathbf{p}_n^{(m)}$ and velocity $\mathbf{v}_n^{(m)}$

$$\mathbf{x}_n^{(m)} = [(\mathbf{p}_n^{(m)})^\top, (\mathbf{v}_n^{(m)})^\top]^\top$$

and the movement of each agent follows as

$$\mathbf{x}_n^{(m)} = \mathbf{F}\mathbf{x}_{n-1}^{(m)} + \mathbf{G}\mathbf{n}_{a,n}^{(m)}$$

with

$$\mathbf{F} = \begin{bmatrix} 1 & 0 & \Delta T & 0 \\ 0 & 1 & 0 & \Delta T \\ 0 & 0 & 1 & 0 \\ 0 & 0 & 0 & 1 \end{bmatrix} \quad \mathbf{G} = \begin{bmatrix} \frac{\Delta T^2}{2} & 0 \\ 0 & \frac{\Delta T^2}{2} \\ \Delta T & 0 \\ 0 & \Delta T \end{bmatrix}$$

where we assume that the driving acceleration noise $\mathbf{n}_{a,n}^{(m)}$ follows a zero-mean, Gaussian distribution (assumed to be independent across m and n) with variance σ_a^2 and ΔT denotes the sample period of n . The individual state vectors of the cooperating agents $m \in \mathcal{M}$ are stacked into a state vector of all agents $\mathbf{x}_n^{\mathcal{M}} = [(\mathbf{x}_n^{(1)})^\top, \dots, (\mathbf{x}_n^{(M)})^\top]^\top$ and the motion model becomes

$$\underbrace{\begin{bmatrix} \mathbf{x}_n^{(1)} \\ \vdots \\ \mathbf{x}_n^{(M)} \end{bmatrix}}_{\mathbf{x}_n^{\mathcal{M}}} = \underbrace{\begin{bmatrix} \mathbf{F} & & \mathbf{0} \\ & \ddots & \\ \mathbf{0} & & \mathbf{F} \end{bmatrix}}_{\mathbf{F}^{\mathcal{M}}} \underbrace{\begin{bmatrix} \mathbf{x}_{n-1}^{(1)} \\ \vdots \\ \mathbf{x}_{n-1}^{(M)} \end{bmatrix}}_{\mathbf{x}_{n-1}^{\mathcal{M}}} + \underbrace{\begin{bmatrix} \mathbf{G} & & \mathbf{0} \\ & \ddots & \\ \mathbf{0} & & \mathbf{G} \end{bmatrix}}_{\mathbf{n}_{a,n}^{\mathcal{M}}} \underbrace{\begin{bmatrix} \mathbf{n}_{a,n}^{(1)} \\ \vdots \\ \mathbf{n}_{a,n}^{(M)} \end{bmatrix}}_{\mathbf{n}_{a,n}^{\mathcal{M}}}. \quad (5)$$

B. Measurement model

The measurement model relates the positions of the agents to delays of deterministic MPCs. Using the predicted agent positions from the motion model, the algorithm calculates a set of expected MPC delays. The expected delays are associated to estimated MPC delays obtained from the measured channel impulse responses. Finally, the employed EKF facilitates the measurement model for updating the agents' positions by consideration of the associated MPC delays.

1) *Estimation of multipath components*: To estimate the delays of the MPCs, each agent performs self and relative channel measurements. An iterative least-squares approximation [28], [29] is used to extract one MPC per iteration ℓ from each measurement $r_n^{(m',m)}(t)$.

Initializing the signal $r^{(\ell)}(t)$ with $r^{(0)}(t) = r_n^{(m',m)}(t)$ the delay $\hat{\tau}_{\ell,n}^{(m',m)}$ of the strongest MPC in $r^{(\ell)}(t)$ is estimated as

$$\hat{\tau}_{\ell,n}^{(m',m)} = \operatorname{argmin}_{\tau} \int_0^T |r^{(\ell)}(t) - a^{(\ell)}(\tau)s(t-\tau)|^2 dt$$

with

$$a^{(\ell)}(\tau) = \int_0^T [s(t-\tau)]^* r^{(\ell)}(t) dt \quad (6)$$

where T denotes the measurement duration. The corresponding amplitude follows as $\hat{a}_{\ell,n}^{(m',m)} = a^{(\ell)}(\hat{\tau}_{\ell,n}^{(m',m)})$. Both

$\hat{\tau}_{\ell,n}^{(m',m)}$ and $\hat{\alpha}_{\ell,n}^{(m',m)}$ are estimated from $r^{(\ell)}(t)$ at each iteration step ℓ , followed by updating $r^{(\ell+1)}(t)$ according to

$$r^{(\ell+1)}(t) = r^{(\ell)}(t) - \hat{\alpha}_{\ell,n}^{(m',m)} s(t - \hat{\tau}_{\ell,n}^{(m',m)})$$

until the $Z_n^{(m',m)}$ strongest MPCs are found.

The estimated MPC delays of each self and relative measurement are multiplied by c to obtain the MPC ranges $\hat{d}_{\ell,n}^{(m',m)} = c\hat{\tau}_{\ell,n}^{(m',m)}$, which are stored in the sets

$$Z_n^{(m',m)} = \left\{ \hat{d}_{\ell,n}^{(m',m)} \right\}_{\ell=1}^{Z_n^{(m',m)}}. \quad (7)$$

2) *Prediction of deterministic MPCs*: Employing the motion model (5) yields the predicted agent positions $\check{\mathbf{p}}_n^{(m)}$ contained in $\check{\mathbf{x}}_n^M = \mathbf{F}^M \mathbf{x}_{n-1}^M$. The expected range of MPC k follows from the geometry model (see Sec. II-B) as

$$d_{k,n}^{(m',m)} = d(\check{\mathbf{p}}_n^{(m')}, \check{\mathbf{p}}_n^{(m)}, \mathbf{s}_k^{(m',m)}), \quad \text{for all } k \in \mathcal{K}_n^{(m',m)}. \quad (8)$$

The set of expected MPCs $\mathcal{K}_n^{(m',m)}$ depends on the agents' positions and the environment. As the propagation of deterministic MPCs is potentially affected by obstacles and neighboring wall segments, we verify their existence using an optical ray-tracer³ [30, p. 132] to obtain the set of deterministic MPCs $\mathcal{K}_n^{(m',m)}$. Finally, we gather the expected ranges in the set

$$\mathcal{D}_n^{(m',m)} = \left\{ d_{k,n}^{(m',m)} : k \in \mathcal{K}_n^{(m',m)} \right\}. \quad (9)$$

3) *Association of expected to deterministic MPCs*: To associate the estimated ranges $Z_n^{(m',m)}$ to expected ranges $\mathcal{D}_n^{(m',m)}$ we use the Munkres algorithm [31] based on an *optimal sub-pattern assignment* metric [32]. The Munkres algorithm aims at associating each expected range $\check{d}_{k,n}^{(m',m)}$ to a measured one $\hat{d}_{\ell,n}^{(m',m)}$. The outcome $\mathcal{A}_n^{(m',m)}$ contains pairs of associated ranges $(\hat{d}_{k,n}^{(m',m)}, \check{d}_{k,n}^{(m',m)})$, labeled by MPC indices $k \in \mathcal{K}_n^{(m',m)}$. Note, that we apply a cut-off distance d_c [29] which limits the discrepancy between each associated pair to a maximum distance, $|\hat{d}_{k,n}^{(m',m)} - \check{d}_{k,n}^{(m',m)}| \leq d_c$. Setting d_c to small values (in sub-meter range) limits the number of potential associations. A higher value enables more associations but also increases the risk of wrong associations (see Sec. IV-F).

After the association, the measured and the expected ranges of each associated pair $(\hat{d}_{k,n}^{(m',m)}, \check{d}_{k,n}^{(m',m)}) \in \mathcal{A}_n^{(m',m)}$ are stacked in the vectors

$$\mathbf{z}_n^{(m',m)} = [\dots, \hat{d}_{k,n}^{(m',m)}, \dots] \quad (10)$$

$$\mathbf{d}_n^{(m',m)} = [\dots, \check{d}_{k,n}^{(m',m)}, \dots]. \quad (11)$$

4) *Update step*: The associated ranges of the self and relative measurements are stacked in the observation vector \mathbf{z}_n according to

$$\mathbf{z}_n = [\mathbf{z}_n^{(1,1)}, \dots, \mathbf{z}_n^{(1,M)}, \mathbf{z}_n^{(2,1)}, \dots, \mathbf{z}_n^{(2,M)}, \dots, \mathbf{z}_n^{(M,M)}]^\top \quad (12)$$

³Application of the ray-tracer to the examples shown in Fig. 9 and 10 yields six and seven deterministic MPCs for the self and relative measurement, respectively, considering first- and second-order reflections.

and the expected ranges in

$$\mathbf{d}_n = [\mathbf{d}_n^{(1,1)}, \dots, \mathbf{d}_n^{(1,M)}, \mathbf{d}_n^{(2,1)}, \dots, \mathbf{d}_n^{(2,M)}, \dots, \mathbf{d}_n^{(M,M)}]^\top$$

both with length $K_n = \sum_{m',m} |\mathcal{A}_n^{(m',m)}|$. The EKF employs the Jacobian \mathbf{H}_n^M of the non-linear function (8) [19] to describe the gradient of the deterministic MPC ranges with respect to the agent positions, evaluated at the predicted agent positions

$$\mathbf{H}_n^M = \left. \frac{\partial h(\mathbf{x}^M)}{\partial \mathbf{x}^M} \right|_{\mathbf{x}^M = \check{\mathbf{x}}_n^M} = \begin{bmatrix} \mathbf{h}_{1,n}^M \\ \vdots \\ \mathbf{h}_{\kappa,n}^M \\ \vdots \\ \mathbf{h}_{K_n,n}^M \end{bmatrix}. \quad (13)$$

Each row $\kappa \in [1, K_n]$ of \mathbf{H}_n^M considers one associated range.

Assuming the κ th row belongs to MPC k obtained at a self measurement of agent m then the range gradient of (8) (derived in Appendix C-1) follows as

$$\dot{\mathbf{d}}_{k,n}^{(m)} = \left. \frac{\partial d(\mathbf{p}^{(m')}, \mathbf{p}^{(m)}, \mathbf{s}_k^{(m',m)})}{\partial \mathbf{p}^{(m)}} \right|_{\mathbf{p}^{(m)} = \check{\mathbf{p}}_n^{(m)}}$$

and the κ th row of \mathbf{H}_n^M is defined as

$$\mathbf{h}_{\kappa,n}^M = \left[0, \dots, \underbrace{(\dot{\mathbf{d}}_{k,n}^{(m)})^\top}_{\text{index } \mu}, \dots, 0 \right] \quad (14)$$

where μ is the index of the m th agent position $\mathbf{p}_n^{(m)}$ within the state vector \mathbf{x}_n^M .

In case that κ belongs to MPC k estimated at a relative measurement between agents m and m' then the range gradients from Appendix C-2 are employed,

$$\dot{\mathbf{d}}_{k,n}^{(m')} = \left. \frac{\partial d(\mathbf{p}^{(m')}, \check{\mathbf{p}}_n^{(m)}, \mathbf{s}_k^{(m',m)})}{\partial \mathbf{p}^{(m')}} \right|_{\mathbf{p}^{(m')} = \check{\mathbf{p}}_n^{(m)'}}$$

$$\dot{\mathbf{d}}_{k,n}^{(m)} = \left. \frac{\partial d(\check{\mathbf{p}}_n^{(m')}, \mathbf{p}^{(m)}, \mathbf{s}_k^{(m',m)})}{\partial \mathbf{p}^{(m)}} \right|_{\mathbf{p}^{(m)} = \check{\mathbf{p}}_n^{(m)}}$$

and the κ th row of \mathbf{H}_n^M follows as

$$\mathbf{h}_{\kappa,n}^M = \left[0, \dots, \underbrace{(\dot{\mathbf{d}}_{k,n}^{(m')})^\top}_{\text{index } \mu}, \dots, \underbrace{(\dot{\mathbf{d}}_{k,n}^{(m)})^\top}_{\text{index } \nu}, \dots, 0 \right]$$

with μ and ν denoting the indices which locate the positions of agents m' and m within \mathbf{x}_n^M , respectively.

C. Range uncertainty estimation

The proposed algorithm uses the MPC-range uncertainty $\text{var}\{\hat{d}_{k,n}^{(m',m)}\}$ to describe the measurement noise \mathbf{n}_n . To estimate the range uncertainties we employ the signal-to-interference-plus-noise ratio (SINR) of the corresponding MPCs which defines the Cramér-Rao lower bound [7], [29]

$$\text{var}\{\hat{d}_{k,n}^{(m',m)}\} \geq \left(\frac{8\pi^2 \beta^2}{c^2} \text{SINR}_{k,n}^{(m',m)} \right)^{-1}$$

with

$$\text{SINR}_{k,n}^{(m',m)} = \frac{|\tilde{\alpha}_{k,n}^{(m',m)}|^2}{N_0 + T_p S_\nu^{(m',m)} (\tilde{\tau}_{k,n}^{(m',m)})}$$

where β is the effective (root mean square) bandwidth and T_p the pulse duration of $s(t)$. The SINR is a function of the MPC amplitudes $\tilde{\alpha}_{k,n}^{(m',m)}$ and the PDP $S_\nu^{(m',m)}(\tau)$ evaluated at MPC delays $\tau = \tilde{\tau}_{k,n}^{(m',m)}$ [7].

As the parameter estimation of MPCs as well as their association to expected ones may be erroneous, especially if only one snapshot of the channel impulse response is available, we propose to employ the geometry model to calculate the MPC delays $\tilde{\tau}_{k,n}^{(m',m)}$ using (2), once the update step of the agents' positions is performed. The corresponding amplitudes $\tilde{\alpha}_{k,n}^{(m',m)}$ are estimated by projection of the received signal on the delayed pulse $s(t - \tilde{\tau}_{k,n}^{(m',m)})$ (equivalent to (6)). Finally, the SINR is estimated using a method-of-moments estimator [29] taking the amplitudes $\{\tilde{\alpha}_{k,i}^{(m',m)}\}_{i=n-N}^{n-1}$ over a window of N past measurements into account.

An alternative way of estimating the measurement noise considers the variance of the differences between the estimated $\hat{d}_{k,n}^{(m',m)}$ and the expected ranges $\tilde{d}_{k,n}^{(m',m)}$ over N past measurements. However, this method can be applied only for MPCs assigned to expected ones. Weak MPCs are unlikely to be discovered at each measurement which may result in a biased variance estimation due to less observation points.

Assuming independence among the measurements the range uncertainties of each self and relative measurement are stacked according to (12) and a diagonal measurement noise covariance matrix follows as

$$\mathbf{R}_n = \text{diag}([\dots, \text{var}\{\hat{d}_{k,n}^{(m',m)}\}, \dots]). \quad (15)$$

D. Incorporation of wall segment uncertainty

The proposed algorithm models the wave propagation employing a geometry model where the MPCs are assumed to be reflected at planar surfaces, e.g. wall segments, whose locations are known. In practice, several violations of the geometry model have to be considered. First, the locations of the wall segments, used for modeling the multipath propagation, are typically provided by building plans with limited accuracy, leading to biased expected MPC delays. Further, wall segments consist of multiple layers of materials, each with different reflection and transmission properties. The reduced propagation speed inside the materials adds a positive bias to the distance estimates.

To address the aforementioned sources of errors we propose to consider the geometry model within the state-space. Inclusion of the wall segments in the state-space allows to recursively update the segment locations using the estimated MPC ranges. Stacking the wall segment locations at time step n in the vector $\mathbf{p}_n^S = [\mathbf{p}_{1,n}^T, \dots, \mathbf{p}_{S,n}^T]^T$ with dimension $(2S \times 1)$ yields the joint state vector consisting of agents and wall segments according to

$$\mathbf{x}_n = [(\mathbf{x}_n^M)^T, (\mathbf{p}_n^S)^T]^T.$$

The covariance of the stacked segment locations is described by

$$\mathbf{P}_n^S = \begin{bmatrix} \mathbf{P}_{1,1,n} & & & \mathbf{P}_{1,S,n} \\ & \ddots & & \\ & & \ddots & \\ \mathbf{P}_{S,1,n} & & & \mathbf{P}_{S,S,n} \end{bmatrix}$$

where $\mathbf{P}_{s,s,n}$ is the covariance of wall segment s and $\mathbf{P}_{s',s,n}$ is the cross-covariance between the segment s' and s . Then, the covariance of the state vector \mathbf{x}_n follows as

$$\mathbf{P}_n = \begin{bmatrix} \mathbf{P}_n^M & \mathbf{P}_n^{M,S} \\ (\mathbf{P}_n^{M,S})^T & \mathbf{P}_n^S \end{bmatrix}$$

with \mathbf{P}_n^M and $\mathbf{P}_n^{M,S}$ being the covariance of the agent state vector \mathbf{x}_n^M and the cross-covariance of agent positions and segment locations, respectively.

The state-space and measurement models are adapted accordingly. Assuming the segments to be static, the state-space model in (5) is extended as follows

$$\begin{aligned} \mathbf{x}_n &= \begin{bmatrix} \mathbf{F}^M & \mathbf{0}_{(4M \times 2S)} \\ \mathbf{0}_{(2S \times 4M)} & \mathbf{0}_{(2S \times 2S)} \end{bmatrix} \mathbf{x}_{n-1} + \begin{bmatrix} \mathbf{n}_{a,n}^M \\ \mathbf{0}_{(2S \times 2)} \end{bmatrix} \\ &= \mathbf{F} \mathbf{x}_{n-1} + \mathbf{n}_{a,n}, \end{aligned} \quad (16)$$

with covariance \mathbf{Q}_n of the process noise $\mathbf{n}_{a,n}$. The measurement model considers the relation between deterministic MPC ranges and wall segment locations. Its Jacobian, evaluated for the predicted state $\check{\mathbf{x}}_n = \mathbf{F} \mathbf{x}_{n-1}$, is defined as (c.f. (13))

$$\mathbf{H}_n = \left. \frac{\partial h(\mathbf{x})}{\partial \mathbf{x}} \right|_{\mathbf{x}=\check{\mathbf{x}}_n} = \begin{bmatrix} \mathbf{h}_{1,n} \\ \vdots \\ \mathbf{h}_{K_n,n} \end{bmatrix}. \quad (17)$$

Assuming the κ th measurement in \mathbf{z}_n belongs to MPC k of the channel between agent m' and m , respectively, then the range gradients with respect to the locations of the segments⁴ $\{\check{\mathbf{p}}_{s,n}\}$ follow as

$$\dot{\mathbf{d}}_{k,s,n} = \left. \frac{\partial d(\check{\mathbf{p}}_n^{(m)}, \check{\mathbf{p}}_n^{(m')}, \mathbf{s}_k^{(m',m)})}{\partial \mathbf{p}_s} \right|_{\mathbf{p}_s = \check{\mathbf{p}}_{s,n}}$$

and row $\mathbf{h}_{\kappa,n}$ is written as

$$\mathbf{h}_{\kappa,n} = [\mathbf{h}_{\kappa,n}^M, \dots, \underbrace{\dot{\mathbf{d}}_{k,1,n}^T}_{\text{index } \eta_1}, \dots, \underbrace{\dot{\mathbf{d}}_{k,I,n}^T}_{\text{index } \eta_I}, \dots]$$

where the indices η_1, \dots, η_I locate the segment indices in $\mathbf{s}_k^{(m',m)}$ within the state vector, and $\mathbf{h}_{\kappa,n}^M$ is defined in (14).

The algorithm includes all wall segment locations $\{\mathbf{p}_{s,n} : s \in \mathcal{S}\}$ in the state vector \mathbf{x}_n in order to take advantage of the correlation with the agents $\mathbf{P}_n^{M,S}$ as well as the correlation inbetween any two wall segments $\mathbf{P}_{s',s,n}$. These correlations spread the obtained information to the neighboring wall segments not assigned to an MPC at n , which is important as the number of associated MPCs K_n is in general small compared to the number of modeled wall segments S .

A summary of the algorithm, including the EKF equations [19], is presented in Algorithm 1.

IV. RESULTS

The proposed algorithm for anchor-less tracking of cooperating agents is based on several simplifications, e.g. the assumption of non-overlapping MPCs to ensure an accurate data association, and the necessity of a reliable building

⁴Note, in (16) the segments are assumed to be static which results in $\check{\mathbf{p}}_{s,n} = \check{\mathbf{p}}_{s,n-1}$ for all s .

Algorithm 1: Summary of the proposed algorithm.

assemble state vector \mathbf{x}_0 , covariance \mathbf{P}_0 , process noise \mathbf{Q}_0 and measurement noise \mathbf{R}_0 using the initialization values from Sec. IV-B

foreach $n > 0$ **do**

 predict state vector $\check{\mathbf{x}}_n = \mathbf{F}\mathbf{x}_{n-1}$
 covariance prediction $\check{\mathbf{P}}_n = \mathbf{F}\mathbf{P}_{n-1}\mathbf{F}^\top + \mathbf{Q}_n$
 foreach measurement between m and m' **do**
 estimate MPC delays $\mathcal{Z}_n^{(m',m)}$; c.f. (7)
 predict deterministic MPC delays $\mathcal{D}_n^{(m',m)}$ at $\check{\mathbf{x}}_n$;
 c.f. (9)
 associate estimated and predicted MPCs resulting
 in $\mathbf{z}_n^{(m',m)}$ and $\mathbf{d}_n^{(m',m)}$; c.f. (10) and (11)
 stack all measurements in \mathbf{z}_n and predictions in \mathbf{d}_n
 compute the Jacobian \mathbf{H}_n at $\check{\mathbf{x}}_n$; c.f. (17)
 estimate measurement noise \mathbf{R}_n ; c.f. (15)
 Kalman gain $\mathbf{K}_n = \check{\mathbf{P}}_n\mathbf{H}_n(\mathbf{H}_n\check{\mathbf{P}}_n\mathbf{H}_n^\top + \mathbf{R}_n)^{-1}$
 state estimate $\hat{\mathbf{x}}_n = \check{\mathbf{x}}_n + \mathbf{K}_n(\mathbf{z}_n - \mathbf{d}_n)$
 covariance estimate $\hat{\mathbf{P}}_n = (\mathbf{I} - \mathbf{K}_n\mathbf{H}_n)\check{\mathbf{P}}_n$
 foreach measurement between m and m' **do**
 foreach MPC $k \in \mathcal{K}_n^{(m',m)}$ **do**
 calculate delay $\{\tilde{r}_{k,n}^{(m',m)}\}$ at $\hat{\mathbf{x}}_n$
 estimate amplitude $\{\tilde{\alpha}_{k,n}^{(m',m)}\}$ and
 measurement noise; c.f. Sec. III-C

floorplan used for the geometry model. Further, the EKF facilitates a linearized measurement model to obtain the estimated agent positions using the measured distances. To validate these simplifications we performed an extensive measurement campaign using several agents in different setups. In Section IV-C we demonstrate the possibility of tracking two agents without anchor information, taking into account wall segment uncertainties. In Section IV-D we evaluate the potential performance gain when also a fixed anchor is available. Finally, in Section IV-E we stress the robustness regarding uncertain floorplans and different signal bandwidths.

A. Setup for measured data

We obtained the measured data using a (maximum length sequence) channel sounder by *Imsens* [33] which spans a bandwidth of 3.5 – 10.5 GHz with an output power (at the antenna) of approx. –40 dBm/MHz. The received impulse response is shaped with a raised-cosine pulse with roll-off factor of $R = 0.6$ at a carrier frequency of $f_c = 7$ GHz [34]. Throughout the experiments in Sections IV-C and IV-D we keep the pulse duration T_p of the raised-cosine pulse fixed at $T_p = 0.5$ ns (corresponding to a 3 dB bandwidth of 2 GHz), while in Sec. IV-E we evaluate the impact of T_p on the algorithm. We use self-made Euro-cent coin antennas [35, p. 86] [36] with approximately uniform radiation patterns in azimuth domain and zeros in the directions of floor and ceiling. Thus, MPCs at floor and ceiling are attenuated by the beampattern. The agents were placed 1.2 m above the floor. To perform the self localization, each agent is equipped with

two antennas, one acting as transmitter and the other one as receiver. We used RF switching matrices [37] to automate the measurements, facilitating up to 4 transmitter and 6 receiver antennas.

B. Implementation and initialization

The algorithm was implemented according to Algorithm 1. The agents' positions are initialized at $n = 0$ with their true⁵ positions. The agents' position covariance is initialized with $\mathbf{P}_0^M = \text{diag}([\sigma_{\text{agent}}^2, \dots, \sigma_{\text{agent}}^2])$ with $\sigma_{\text{agent}}^2 = 0.03^2$ m², the wall segment uncertainties are initialized with $\{\mathbf{P}_{s,s,0} = \text{diag}([\sigma_{\text{seg}}^2, \sigma_{\text{seg}}^2]) : s \in \mathcal{S}\}$ and $\sigma_{\text{seg}}^2 = 0.003^2$ m², and the cross-correlations $\mathbf{P}_0^{M,S}$ and $\mathbf{P}_{s',s,0}$ are initialized with zeros (for all $s', s \in \mathcal{S} : s' \neq s$). The driving noise σ_a^2 is set according to the maximum agent velocity of $\|\mathbf{v}_{\text{max}}\| = 0.025$ m/step such that $\sigma_a^2 = (\|\mathbf{v}_{\text{max}}\|/(3\Delta T))^2$ with $\Delta T = 1$ step. The measurement noise is initialized with $\mathbf{R}_0 = \text{diag}([0.07^2, \dots, 0.07^2])$ m².

The expected number of MPCs $|\mathcal{K}_n^{(m',m)}|$ depends on the agents' positions and the room geometry (see Sec. III-B2). The number of deterministic first-order reflections in the received signals is in the order of four to six whereas hundreds of higher-order reflections can be found. However, higher-order reflections are strongly affected by path overlap, resulting in challenging data association. Thus, the geometry model considers first- and second-order MPCs only.

We set the cut-off distance (c.f. Sec. III-B3) to $d_c = cT_p$ and the number of estimated MPCs $Z_n^{(m',m)}$ (Sec. III-B1) to $Z_n^{(m',m)} = 1.5|\mathcal{K}_n^{(m',m)}|$. MPC pairs whose expected ranges are equal within the cut-off distance d_c are not considered in (8) for avoiding wrong data associations. For the MPCs' range uncertainty estimation (see Sec. III-C), the algorithm considers past measurements received within a distance (along the agent track) of 0.2 m.

C. Proof-of-concept experiment

We first present a proof-of-concept experiment. We are interested in how the algorithm gathers information necessary for tracking without the use of anchors. Further, we stress its robustness of dealing with a bias in the provided floorplan.

The agent network consists of two agents $m \in \{1, 2\}$ moving along trajectories of $n \in \{1, \dots, 200\}$ with velocity 2.5 cm/step, as shown in Fig. 2. The floorplan considers planar surfaces, e.g. concrete walls, doors, windows. To limit the number of deterministic MPCs, we consider wall segments of a length $l_s > 0.25$ m resulting in 71 modeled wall segments. At each n , two self-measurements and one relative measurement are performed. The estimated and associated MPCs are illustrated for $n = 90$.

1) *Reliability of MPCs:* Fig. 3 illustrates the SINRs of the LOS and first-order MPCs bounced at wall segments $\{s_i : i = 1, \dots, 8\}$, respectively. The SINRs reveal information regarding the reliability of the MPCs used in the tracking filter (c.f. Sec. (III-C)). We can observe that the LOS serves as an important component justified by its high SINR. The

⁵The true position was obtained using a measuring tape whose limited accuracy may introduce an error in the range of 1 cm.

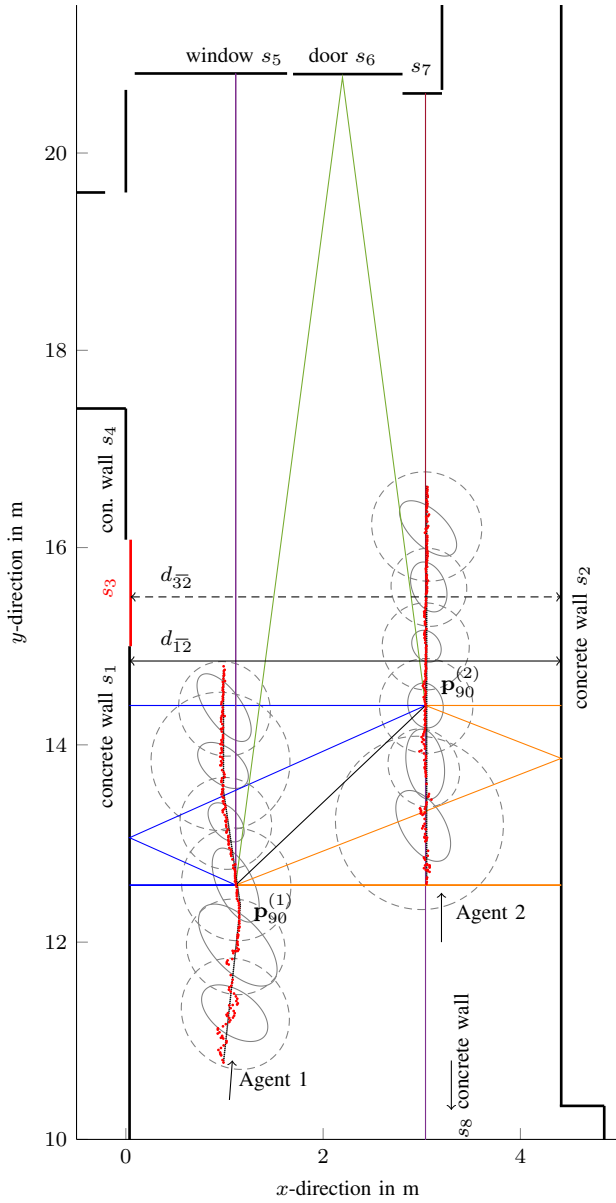


Fig. 2. Proof of concept scenario: Two agents move independently along the trajectories (dotted, black) and estimate their positions (dotted, red). The proposed algorithm tracks the agents by exploiting MPC delays and corresponding SINRs (see Fig. 3). Measured and associated MPCs are illustrated for time step $n = 90$. The ellipses illustrate the standard deviation of the position estimates before (dashed, scaled by a factor of 10) and after the update step (solid, scaled by a factor of 40) at $n = \{30, 60, \dots, 180\}$.

reflections at concrete walls $\{s_1, s_2, s_4, s_7, s_8\}$, doors $\{s_3, s_6\}$ and the window $\{s_5\}$ are also promising candidates although their SINRs are lower compared to the LOS.

Both agents are closely surrounded by walls along the x -direction whereas the y -direction provides more space. In general, closely-located wall segments result in stronger MPCs which are valuable for positioning. This observation translates to a lower standard deviation of the position error along the x -direction, illustrated by the ellipses in Fig. 2.

2) *Floorplan inaccuracies*: As the proposed algorithm facilitates deterministic MPCs, its performance is strongly dependent on the accuracy of the provided floorplan. We

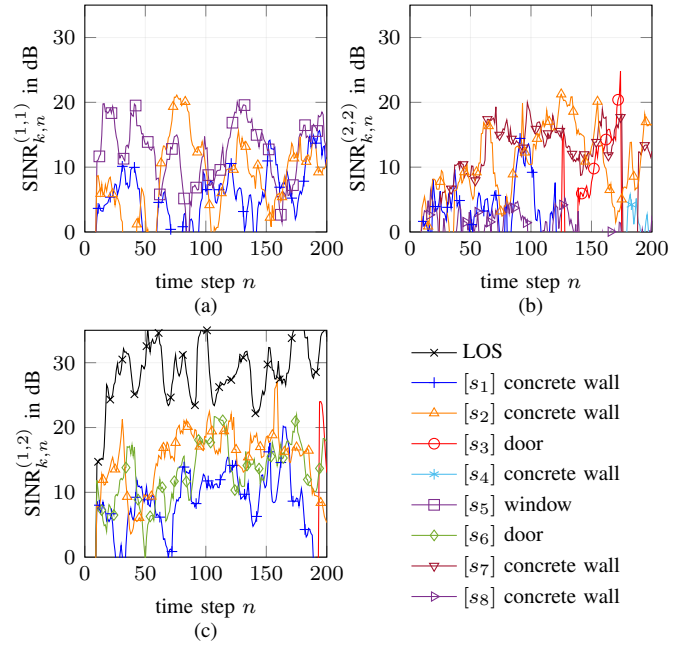


Fig. 3. Estimated SINR-values obtained from agent one's (a) and agent two's (b) self measurements, respectively, and from relative measurements between both agents (c). The associated wall segments in $s_k^{(m',m)}$ and corresponding multipath propagation paths are illustrated in Fig. 2. High SINR-values indicate a reliable MPC range measurement. The range of the LOS is most accurate, justified by its high SINR.

can consider two challenges: (i) the electromagnetic waves experience a different floorplan due to effects like diffraction and penetration and (ii) the provided floorplan is inaccurate, e.g. pin boards mounted on the wall segments are not considered. The algorithm cannot distinguish between both cases. It employs the estimated MPC parameters to recursively update the floorplan. At each time step n the EKF weighs between the prior segment location and the measured MPC ranges using the prior covariance and the measurement noise. Each measured MPC provides location information to the floorplan. We are interested in the impact of prior location information on the convergence behavior of the floorplan. Figure 4 exemplifies the distance d_{32} between wall segments s_3 and s_2 (see Fig. 2) in comparison with the distance d_{12} between the wall segments s_1 and s_2 along n . According to the building floorplan, both s_1 and s_3 are in-line, resulting in $d_{32} \approx d_{12}$.

We initialized the location of s_3 with a bias of 0.1 m along its x -direction and analyze the rate of convergence using different initializations of the segment uncertainty σ_{seg} , namely $\sigma^* = 10$ mm, $\sigma^\circ = 3$ mm, and $\sigma^\diamond = 1$ mm, resulting in distances d_{32}^* , d_{32}° and d_{32}^\diamond , respectively. Wall segments s_1 and s_2 are associated to MPC measurements, starting with $n = 1$ and the distance between both segments attains $d_{12} \approx 4.38$ m. At time steps $n \in \{120, \dots, 175\}$, an MPC from segment s_3 is discovered in Agent 2's self measurement. Immediately the segment location is rearranged such that the expected MPC range matches with the measured one and d_{32} converges to d_{12} . Figure 4 (b) exemplifies the standard deviation $([\mathbf{P}_{3,3,n}]_x)^{\frac{1}{2}}$ of wall segment s_3 along its x -direction. The more estimated MPCs are associated to s_3 , the lower gets its variance. We

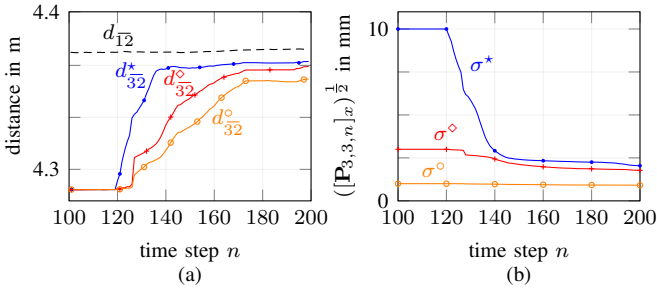


Fig. 4. Adaptation of floorplan dependent on the initialized wall segment uncertainty. The rate of convergence of the distance between s_2 and s_3 for different initializations of uncertainty $\sigma^* = 10$ mm, $\sigma^\circ = 3$ mm and $\sigma^\circ = 1$ mm results in convergence rates d_{32}^* , d_{32}° and d_{32}° . Higher uncertainties (b) lead to a faster floorplan adaption (a).

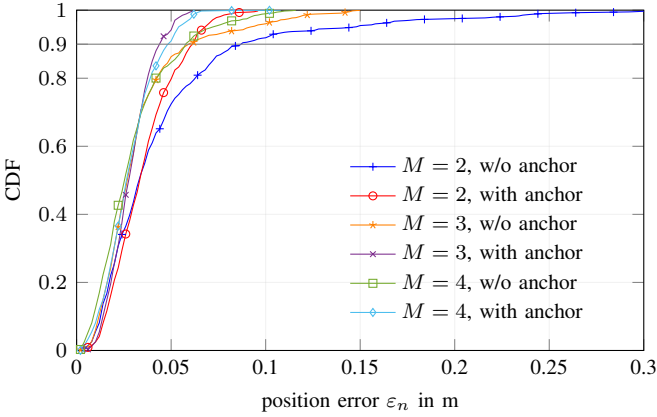


Fig. 5. CDF of the agent's position error for different number $M \in \{2, 3, 4\}$ of cooperating agents with and without anchor for $T_p = 0.5$ ns.

can observe that a high prior uncertainty of σ^* enables a fast adaption of the wall segment location and the initial bias is reduced. If the wall segment prior uncertainty is lowered (σ°) then the EKF relies more on the prior locations and the convergence rate is reduced.

D. Impact of anchor and number of agents

To evaluate the benefit of a fixed anchor we introduce M cooperating agents plus one anchor at position $\mathbf{p}^{(a)}$, as illustrated in Fig. 7. The agents move independently along their trajectories of $n \in \{1, \dots, 200\}$ with varying velocities of 1 – 2.5 cm/step and perform, in summary, M self and $M(M-1)/2$ relative measurements at each n . Additionally, each agent runs one relative measurement to the fixed anchor. These measurements are treated in the same manner as the relative measurements between the agents. The transmitting agent in (2) is set to the anchor's position ($\mathbf{p}^{(m')} = \mathbf{p}^{(a)}$) and the additional measurement equations $\{\tau_{k,n}^{(a,m)}\}$, for all k, m are added to (13).

We are interested in the performance in terms of position error for different sizes of the agent network, $M = \{2, 3, 4\}$, with and without the use of an additional fixed anchor. Figure 5 illustrates the cumulative distribution functions (CDFs) of the position error $\varepsilon_n = \sum_m \|\hat{\mathbf{p}}_n^{(m)} - \mathbf{p}_n^{(m)}\|$ with $\mathbf{p}_n^{(m)}$ as true

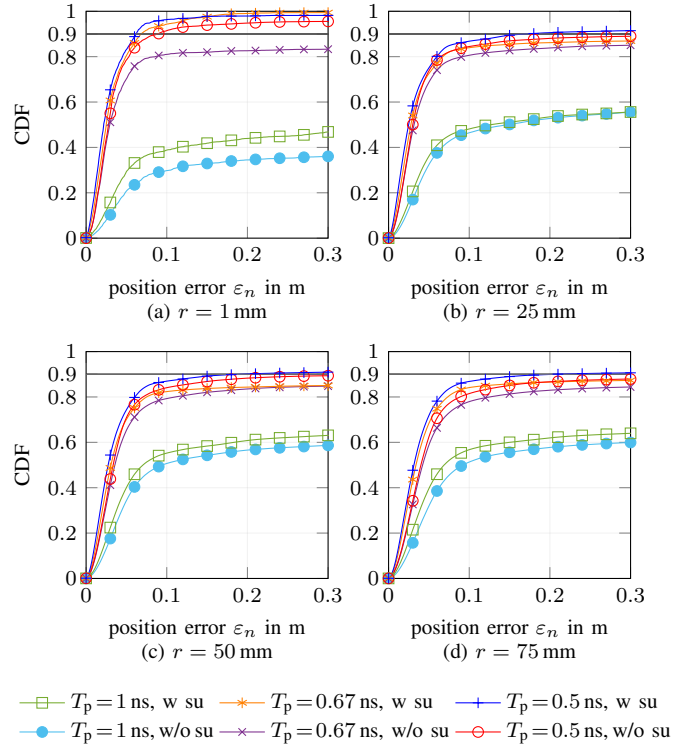


Fig. 6. CDF of the position error using different ranges of floorplan errors of $r = 1$ mm (a), $r = 25$ mm (b), $r = 50$ mm (c) and $r = 75$ mm (d) against pulse duration $T_p \in \{1, 0.67, 0.5\}$ ns, with segment update (w su) and without segment update (w/o su).

position of agent m . It can be observed that the presence of a fixed anchor improves the position error, especially for a small agent network of $M = 2$ which is justified by the higher number of available channel measurements (for $M = 2$, five channel measurements are available with anchor information compared to three channel measurements without). An increasing network size decreases the position error. The performance for $M = 3$ and $M = 4$ is similar but with a slight decrease for $M = 4$ due to NLOS conditions of Agent 4 (see Fig. 7). We can conclude that the algorithm is capable of tracking the agents' positions with only a minor degradation of the position error if no fixed anchor is used.

E. Impact of floorplan accuracy and signal bandwidth

As the algorithm relies strongly on the provided floorplan, we investigate further the impact of an inaccurate floorplan. Therefore, we initialized the locations $\{\mathbf{p}_{s,n} : s \in \mathcal{S}\}$ at $n = 0$ by adding independent, uniformly distributed noise samples to the true locations \mathbf{p}_s

$$\mathbf{p}_{s,0} = \mathbf{p}_s + \mathbf{n}_s, \text{ for all } s \in \mathcal{S}.$$

The elements in \mathbf{n}_s have been sampled from $\mathcal{U}(-r/2, r/2)$ with range r . Further, we are interested in the impact of the pulse duration T_p of the transmitted signal on the position accuracy. The proposed algorithm utilizes MPC parameters whose estimation is biased in case of overlapping MPCs and affected by diffuse multipath propagation. To ensure resolvable

MPCs in the time domain, short pulse duration (corresponding to high bandwidths) are beneficial.

In the following, we compare the proposed algorithm with and without consideration of the segment uncertainty using \mathbf{x}_n and \mathbf{x}_n^M , respectively. We propose to evaluate the agents' position error relative to the floorplan. We consider the loss of an absolute coordinate system if the segment locations are included in the state vector by introducing a center of gravity of the floorplan

$$\hat{\mathbf{p}}_n^g = \left(\sum_{s \in \mathcal{S}} \hat{\mathbf{P}}_{s,s,n}^{-1} \right)^{-1} \sum_{s \in \mathcal{S}} \hat{\mathbf{P}}_{s,s,n}^{-1} \hat{\mathbf{p}}_{s,n}.$$

The center of gravity $\hat{\mathbf{p}}_n^g$ can be interpreted as weighted average of the floorplan feature locations. Uncertain wall segments (indicated by a large covariance $\{\hat{\mathbf{P}}_{s,s,n}\}$) will be less considered in $\hat{\mathbf{p}}_n^g$. The agents' position errors (relative to the floorplan) follow from

$$\varepsilon_n = \sum_m \left\| \left(\hat{\mathbf{p}}_n^{(m)} - \mathbf{p}_n^{(m)} \right) - \left(\hat{\mathbf{p}}_n^g - \mathbf{p}_0^g \right) \right\|$$

where the vector $(\hat{\mathbf{p}}_n^g - \mathbf{p}_0^g)$ accounts for the floorplan adaptation. To obtain the agent positions relative to the floorplan, the movement of $\hat{\mathbf{p}}_n^g$ is subtracted from the position error. We evaluate different levels of floorplan uncertainties $r \in \{1, 25, 50, 75\}$ mm and pulse duration $T_p \in \{0.5, 0.67, 1\}$ ns, each with 100 Monte Carlo runs. Figure 6 illustrates the CDFs of the position error, averaged for agent network sizes of $M = 2, 3$ and 4.

The position error depends strongly on the pulse duration seen by a poor performance at $T_p = 1$ ns. At smaller pulse duration, $T_p \in \{0.67, 0.5\}$ ns, the algorithm performs better because the MPCs tend to be more separated in the time domain yielding a more reliable MPC parameter estimation and association.

In general, we can observe that the position error degrades when a biased floorplan is initialized. This leads to a biased geometry model and subsequently to a challenging association of measured and predicted MPC delays. Including the floorplan in the state-space (using \mathbf{x}_n) enables to remedy the bias in order to get a more consistent floorplan.

F. Discussion and remarks

The algorithm requires to set the initial uncertainty of agents and wall segment locations at $n = 0$. At each time step the EKF updates the agent positions and segment locations by weighing between prior information (from the prediction step) and measured MPC delays associated to measurement noise. A wall segment which is uncertain about its location is more affected by the update step than a certain one (see Fig. 4). In [19, p. 317] the initialization of $\sigma_{\text{seg}}^2 \rightarrow \infty$ is proposed in order to enable a fast adaption. In this case the algorithm relies strongly on the MPC delay measurements and the quality of their data association. We prefer a low value of $\sigma_{\text{seg}}^2 = 0.003^2 \text{ m}^2$ since a slow adaption is more robust to noisy delay measurements and wrong data associations.

We do not add process noise to the segment locations. Each measured MPC thus reduces the segment location uncertainty

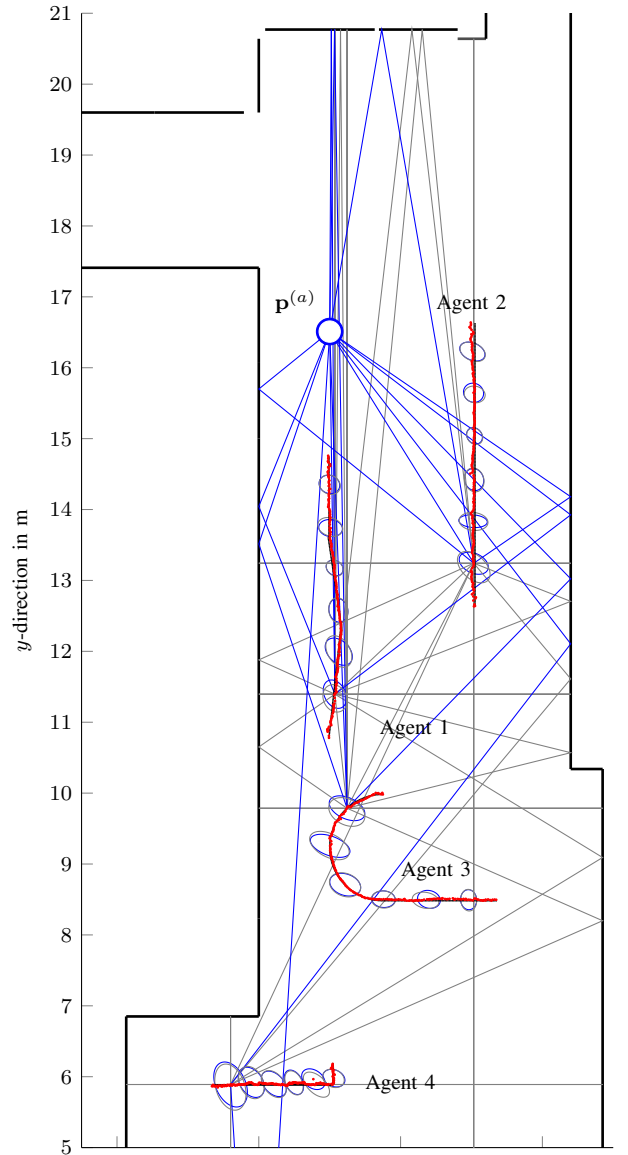


Fig. 7. Illustration of floorplan and agent movement. The agents track their positions (dotted, red) using multipath propagation (gray). Obtaining additional information from a fixed anchor (blue) at $\mathbf{p}^{(a)}$ improves the accuracy, as shown in Fig. 5. The ellipses illustrate the standard deviation of the position estimate with (blue) and without anchor information (gray), scaled by a factor of 40 at $n = \{30, 60, \dots, 180\}$.

(see Fig. 4). Low values of uncertainty prohibit a further adaption and thus a limitation of the lower variance may be useful to keep the adaption active. However, in this work we are interested in how the adaption of the floorplan can be beneficial and we did not implement such a limit.

The data association step is performed using the predicted agent positions. An increased accuracy of the predicted positions yields an increased quality in the data association as well. We recognized that a small cut-off distance between expected and estimated ranges of $d_c = 0.15$ m (at $T_p = 0.5$ ns) is vital when the agent network is off track. A mismatch between predicted and true agent positions yields wrong data associations. As shown in [38], the limitation of the maximum offset to d_c lowers wrong associations.

At the EKF prediction step the covariance of the agents is increased by the driving acceleration noise (with variance σ_a^2). In order to track trajectories with abrupt changes we set the $3\sigma_a$ point equal to the maximum velocity $\|\mathbf{v}_{\max}\| = 0.025$ m/step. We recognized that a smaller driving acceleration noise improves the accuracy but the algorithm was no longer able to follow abrupt turns in the trajectory as it puts too much importance on the motion model. We evaluated the algorithm in a static scenario where the only moving objects are the agents. In a non-static environment, additional (untracked) objects are present which deteriorate the multipath propagation. Subsequently, the SINRs of the MPCs are lowered, the algorithm relies less on MPC delays, and the position estimation uncertainty is increased. In this work, we did not evaluate the importance of static environments.

The complexity of the algorithm is mainly determined by the number of agents M . Considering all agents are located within their communication range then each additional agent requires M channel measurements (Sec. III-B1), range predictions (Sec. III-B2), data associations (Sec. III-B3), and range uncertainty estimations (Sec. III-C). The EKF matrix inversion has a complexity of $\mathcal{O}((MK)^{2.4})$ [19, p. 43] with K as average number of associated MPCs (in practice approx. 4 – 6) and the complexity of the EKF matrix multiplication scales quadratically with the size of the state vector.

Ensuring high localization accuracy goes hand in hand with high synchronization accuracy. At self measurements the transmitter is co-located with the receiver which enables the usage of the same clock. At relative measurements transmitter and receiver are spatially separated and synchronization of the clocks is necessary. Any synchronization error will be reflected in a biased MPC parameter estimation. In literature, strategies to cope or neglect its impact have been proposed, e.g. joint positioning and synchronization [39], or a two-way exchange of pilot sequences like in IEEE 802.15.4a UWB radios [40] or using differential timing information inbetween MPCs [7]. In this work we omit the required synchronization by wiring the antennas to the channel sounder. State of the art UWB radios [40] induce a synchronization error with variance of 5^2 cm² which will affect the presented localization accuracy in a comparable range.

V. CONCLUSIONS

In this paper, we have presented a centralized, cooperative tracking algorithm for wireless networks without the need for further infrastructure, e.g. fixed anchors. We have developed an algorithm based on an extended Kalman filter which makes use of position-related information contained in measured channel impulse responses. To address uncertainties in the environment model we have included the floorplan in the state-space model. The performance evaluation with measured data has shown the feasibility of using deterministic MPCs to simultaneously track absolute agent positions and adapt the floorplan without employing information from an inertial measurement unit or from fixed anchors. The results demonstrate the necessity of high signal bandwidths exceeding 1GHz to prevent overlapping of deterministic MPCs in an indoor environment. Our future

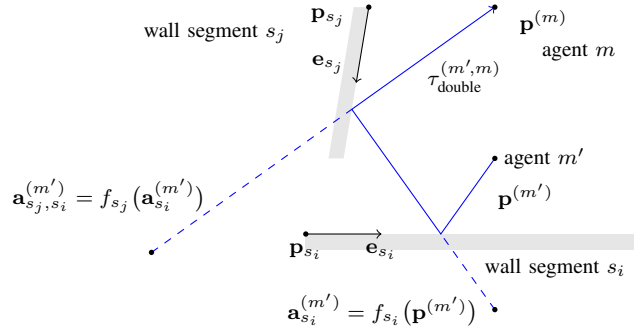


Fig. 8. Illustration of multipath propagation using an image-source model. The position of the transmitting agent m' is mirrored at wall segments s_i and s_j , respectively, to obtain $\mathbf{a}_{s_j, s_i}^{(m')}$.

work will address the reduction of the required bandwidth, the derivation of distributed tracking filters as well as the exploration of additional features in the geometry model.

APPENDIX A DERIVATION OF THE GEOMETRY MODEL

We describe the path of a deterministically modeled MPC k as a function of the positions of the transmitting agent m' , the receiving agent m , and the reflected surfaces. Each MPC is associated to a vector $\mathbf{s}_k^{(m', m)}$ consisting of the indices of the reflecting wall segments in chronological order $\mathbf{s}_k^{(m', m)} = [\dots, s_i, s_j, \dots, s_I]$ where I is the reflection order. Each wall segment $s \in \mathcal{S}$ is described by its location \mathbf{p}_s and alignment \mathbf{e}_s , as illustrated in Fig. 8. The transmitted signal from agent m' is reflected at the wall segments s_i and s_j and finally received by agent m . To calculate the delay of the MPC, an image-source model is used which mirrors the position of the transmitting agent at each reflecting wall segment to obtain mirrored images of the agent position.

Application of the image-source model for a first-order MPC is equivalent with mirroring the position $\mathbf{p}^{(m')}$ at segment $s \in \mathcal{S}$ [16], [41]

$$\begin{aligned} \mathbf{a}_s^{(m')} &= \mathbf{p}^{(m')} - 2\mathbf{T}_s(\mathbf{p}^{(m')} - \mathbf{p}_s) \\ &= (\mathbf{I} - 2\mathbf{T}_s)\mathbf{p}^{(m')} + 2\mathbf{T}_s\mathbf{p}_s \end{aligned} \quad (18)$$

with $\mathbf{T}_s = \mathbf{U}_{\frac{\pi}{2}}\mathbf{e}_s\mathbf{e}_s^T\mathbf{U}_{\frac{\pi}{2}}^T$ and $\mathbf{U}_{\frac{\pi}{2}}$ is a rotation matrix by $\pi/2$ (i.e. $\mathbf{U}_{\frac{\pi}{2}} = [[0, 1]^T, [-1, 0]^T]$). In (18) the matrix multiplication with \mathbf{T}_s extracts the component of $(\mathbf{p}^{(m')} - \mathbf{p}_s)$ which is orthogonal to \mathbf{e}_s . Under the assumption that the segment's location \mathbf{p}_s and alignment \mathbf{e}_s are fixed, the terms $(\mathbf{I} - 2\mathbf{T}_s)$ (denoted as *Householder matrix*) and $2\mathbf{T}_s\mathbf{p}_s$ can be calculated beforehand. Rewriting (18) as a function depending on the agent's position yields the affine transformation

$$\mathbf{a}_s^{(m')} = f_s(\mathbf{p}^{(m')}).$$

Higher-order reflections are modeled straight forwardly. Each reflecting segment is equipped with a virtual source, as shown in Fig. 8. The virtual source $\mathbf{a}_{s_i}^{(m')} = f_{s_i}(\mathbf{p}^{(m')})$, corresponding to segment s_i , is mirrored at segment s_j to obtain

$\mathbf{a}_{s_i, s_j}^{(m')} = f_{s_j}(\mathbf{a}_{s_i}^{(m')})$, which again can be expressed as a function of the agent's position according to

$$\mathbf{a}_{s_i, s_j}^{(m')} = f_{s_j}(f_{s_i}(\mathbf{p}^{(m')})) = f_{s_j} \circ f_{s_i}(\mathbf{p}^{(m')}).$$

The resulting MPC delay $\tau_{\text{double}}^{(m', m)}$ is calculated as norm of the geometric distance between $\mathbf{a}_{s_i, s_j}^{(m')}$ and the receiver position $\mathbf{p}^{(m)}$, scaled by the speed of light c

$$\tau_{\text{double}}^{(m', m)} = \frac{1}{c} \|\mathbf{p}^{(m)} - \mathbf{a}_{s_i, s_j}^{(m')}\|.$$

These steps can be generalized for an arbitrary deterministic MPC delay by considering the reflected segments $\mathbf{s}_k^{(m', m)} = [s_1, \dots, s_I]$ in the function composition of $\{f_s : s \in \mathbf{s}_k^{(m', m)}\}$ according to

$$\tau_k^{(m', m)} = \frac{1}{c} \|\mathbf{p}^{(m)} - (f_{s_I} \circ \dots \circ f_{s_1})(\mathbf{p}^{(m')})\| \quad (19)$$

denoted as measurement equation

$$\tau_k^{(m', m)} = \frac{1}{c} d(\mathbf{p}^{(m')}, \mathbf{p}^{(m)}, \mathbf{s}_k^{(m', m)}) \quad (20)$$

which relates the delay of MPC k to the agents' positions $\mathbf{p}^{(m)}$ and $\mathbf{p}^{(m')}$.

The advantage of using (20) is that the MPC delays are being decomposed into the positions of the agents m and m' and the geometry of the wall segments. It was constructed by mirroring agent position $\mathbf{p}^{(m')}$ at wall segments s_i followed by s_j . In the following (Appendix B) we show for the general case that this procedure is equal to mirroring agent position $\mathbf{p}^{(m)}$ first by s_j followed by s_i and thus, (20) is capable of describing the delay gradients w.r.t both agent positions. In Appendix C we illustrate regularly occurring MPCs and their impact on the positioning algorithm.

APPENDIX B CHANNEL RECIPROCITY

The proposed geometric model distinguishes between the transmitting and receiving agents located at $\mathbf{p}^{(m')}$ and $\mathbf{p}^{(m)}$, respectively. In the following, we show that the MPC delays and the delay gradients with respect to both agents and the floorplan features can be calculated irrespective of which agent is transmitting or receiving. To give a general proof, we show that the measurement equation (20) complies with

$$d(\mathbf{p}^{(m')}, \mathbf{p}^{(m)}, \mathbf{s}_k^{(m', m)}) = d(\mathbf{p}^{(m)}, \mathbf{p}^{(m')}, \mathbf{s}_k^{(m, m')}). \quad (21)$$

The ordering of reflected wall segments is different and needs to be considered. Let $\mathbf{s}_k^{(m', m)}$ consist of the indices of bounced walls of the traveling wave in chronological order (i.e. the i th element $[\mathbf{s}_k^{(m', m)}]_i$ denotes the i th bounced wall) from agent m' to m . Then $\mathbf{s}_k^{(m, m')}$ contains the bounced wall segments in reversed order of $\mathbf{s}_k^{(m', m)}$

$$[\mathbf{s}_k^{(m', m)}]_i = [\mathbf{s}_k^{(m, m')}]_{I-i+1} \quad \text{for all } i = 1, \dots, I. \quad (22)$$

We abbreviate $\mathbf{s}_i^{\triangleright} = [\mathbf{s}_k^{(m', m)}]_i$, $\mathbf{s}_i^{\triangleleft} = [\mathbf{s}_k^{(m, m')}]_i$ and omit the MPC index k for a shorter notation. Plugging (19) in (21) and tacking the square yields

$$\begin{aligned} \frac{1}{c} \left\| \underbrace{\mathbf{p}^{(m)}}_a - \underbrace{\prod_{i=1}^I \mathbf{A}_{\mathbf{s}_i^{\triangleright}} \mathbf{p}^{(m')}}_{-b} - \underbrace{\sum_{i=1}^I \prod_{j=i+1}^I \mathbf{A}_{\mathbf{s}_j^{\triangleright}} \mathbf{b}_{\mathbf{s}_i^{\triangleright}}}_{-c} \right\|^2 = \\ \frac{1}{c} \left\| \underbrace{\mathbf{p}^{(m')}}_d - \underbrace{\prod_{i=1}^I \mathbf{A}_{\mathbf{s}_i^{\triangleleft}} \mathbf{p}^{(m)}}_{-e} - \underbrace{\sum_{i=1}^I \prod_{j=i+1}^I \mathbf{A}_{\mathbf{s}_j^{\triangleleft}} \mathbf{b}_{\mathbf{s}_i^{\triangleleft}}}_{-f} \right\|^2 \end{aligned} \quad (23)$$

with the Householder matrix $\mathbf{A}_{\mathbf{s}_i^{\triangleright}} = (\mathbf{I} - 2\mathbf{T}_{\mathbf{s}_i^{\triangleright}})$ and $\mathbf{b}_{\mathbf{s}_i^{\triangleright}} = 2\mathbf{T}_{\mathbf{s}_i^{\triangleright}} \mathbf{p}_{\mathbf{s}_i^{\triangleright}}$. Rewriting (23) and omitting c results in

$$\|\mathbf{a} + \mathbf{b} + \mathbf{c}\|^2 = \|\mathbf{d} + \mathbf{e} + \mathbf{f}\|^2$$

$$\begin{aligned} \mathbf{a}^T \mathbf{a} + \mathbf{b}^T \mathbf{b} + \mathbf{c}^T \mathbf{c} + 2\mathbf{a}^T \mathbf{b} + 2\mathbf{a}^T \mathbf{c} + 2\mathbf{b}^T \mathbf{c} = \\ \mathbf{d}^T \mathbf{d} + \mathbf{e}^T \mathbf{e} + \mathbf{f}^T \mathbf{f} + 2\mathbf{d}^T \mathbf{e} + 2\mathbf{d}^T \mathbf{f} + 2\mathbf{e}^T \mathbf{f}. \end{aligned}$$

The Householder matrix has the property

$$\begin{aligned} \mathbf{A}_{\mathbf{s}_i^{\triangleright}}^T \mathbf{A}_{\mathbf{s}_i^{\triangleright}} &= (\mathbf{I} - 2\mathbf{U}_{\frac{\pi}{2}} \mathbf{e}_{\mathbf{s}_i^{\triangleright}} \mathbf{e}_{\mathbf{s}_i^{\triangleright}}^T \mathbf{U}_{\frac{\pi}{2}}^T)^T (\mathbf{I} - 2\mathbf{U}_{\frac{\pi}{2}} \mathbf{e}_{\mathbf{s}_i^{\triangleright}} \mathbf{e}_{\mathbf{s}_i^{\triangleright}}^T \mathbf{U}_{\frac{\pi}{2}}^T) \\ &= (\mathbf{I} - 4\mathbf{U}_{\frac{\pi}{2}} \mathbf{e}_{\mathbf{s}_i^{\triangleright}} \mathbf{e}_{\mathbf{s}_i^{\triangleright}}^T \mathbf{U}_{\frac{\pi}{2}}^T + 4\mathbf{U}_{\frac{\pi}{2}} \mathbf{e}_{\mathbf{s}_i^{\triangleright}} \mathbf{e}_{\mathbf{s}_i^{\triangleright}}^T \mathbf{e}_{\mathbf{s}_i^{\triangleright}} \mathbf{e}_{\mathbf{s}_i^{\triangleright}}^T \mathbf{U}_{\frac{\pi}{2}}^T) \\ &= \mathbf{I} \end{aligned} \quad (24)$$

which results in $\mathbf{a}^T \mathbf{a} = \mathbf{e}^T \mathbf{e} = (\mathbf{p}^{(m)})^T \mathbf{p}^{(m)}$ and $\mathbf{b}^T \mathbf{b} = \mathbf{d}^T \mathbf{d} = (\mathbf{p}^{(m')})^T \mathbf{p}^{(m')}$. Using the property

$$\begin{aligned} \mathbf{A}_{\mathbf{s}_i^{\triangleright}} \mathbf{b}_{\mathbf{s}_i^{\triangleright}} &= (\mathbf{I} - 2\mathbf{U}_{\frac{\pi}{2}} \mathbf{e}_{\mathbf{s}_i^{\triangleright}} \mathbf{e}_{\mathbf{s}_i^{\triangleright}}^T \mathbf{U}_{\frac{\pi}{2}}^T) 2\mathbf{U}_{\frac{\pi}{2}} \mathbf{e}_{\mathbf{s}_i^{\triangleright}} \mathbf{e}_{\mathbf{s}_i^{\triangleright}}^T \mathbf{U}_{\frac{\pi}{2}}^T \mathbf{p}_{\mathbf{s}_i^{\triangleright}} \\ &= -2\mathbf{U}_{\frac{\pi}{2}} \mathbf{e}_{\mathbf{s}_i^{\triangleright}} \mathbf{e}_{\mathbf{s}_i^{\triangleright}}^T \mathbf{U}_{\frac{\pi}{2}}^T \mathbf{p}_{\mathbf{s}_i^{\triangleright}} \\ &= -\mathbf{b}_{\mathbf{s}_i^{\triangleright}} \end{aligned}$$

and (24), term $\mathbf{c}^T \mathbf{c}$ results in

$$\begin{aligned} \mathbf{c}^T \mathbf{c} &= \mathbf{b}_{\mathbf{s}_1^{\triangleright}}^T \mathbf{A}_{\mathbf{s}_2^{\triangleright}}^T \cdots \mathbf{A}_{\mathbf{s}_I^{\triangleright}}^T \mathbf{A}_{\mathbf{s}_I^{\triangleright}} \cdots \mathbf{A}_{\mathbf{s}_2^{\triangleright}} \mathbf{b}_{\mathbf{s}_1^{\triangleright}} + \dots \\ &\quad + \mathbf{b}_{\mathbf{s}_I^{\triangleright}}^T \mathbf{A}_{\mathbf{s}_I^{\triangleright}} \cdots \mathbf{A}_{\mathbf{s}_2^{\triangleright}} \mathbf{b}_{\mathbf{s}_I^{\triangleright}} + \dots + \mathbf{b}_{\mathbf{s}_I^{\triangleright}}^T \mathbf{b}_{\mathbf{s}_I^{\triangleright}} \\ &= \mathbf{b}_{\mathbf{s}_1^{\triangleright}}^T \mathbf{b}_{\mathbf{s}_1^{\triangleright}} + \dots - \mathbf{b}_{\mathbf{s}_I^{\triangleright}}^T \mathbf{A}_{\mathbf{s}_{I-1}^{\triangleright}} \cdots \mathbf{A}_{\mathbf{s}_2^{\triangleright}} \mathbf{b}_{\mathbf{s}_I^{\triangleright}} + \dots + \mathbf{b}_{\mathbf{s}_I^{\triangleright}}^T \mathbf{b}_{\mathbf{s}_I^{\triangleright}}. \end{aligned}$$

Since the first bounced wall in $\mathbf{s}_i^{\triangleleft}$ equals the last bounced wall in $\mathbf{s}_i^{\triangleright}$, $\mathbf{s}_i^{\triangleleft} = \mathbf{s}_{I-i+1}^{\triangleright}$, the term $\mathbf{f}^T \mathbf{f}$ follows as

$$\begin{aligned} \mathbf{f}^T \mathbf{f} &= \mathbf{b}_{\mathbf{s}_I^{\triangleleft}}^T \mathbf{A}_{\mathbf{s}_{I-1}^{\triangleleft}}^T \cdots \mathbf{A}_{\mathbf{s}_1^{\triangleleft}}^T \mathbf{A}_{\mathbf{s}_1^{\triangleleft}} \cdots \mathbf{A}_{\mathbf{s}_{I-1}^{\triangleleft}} \mathbf{b}_{\mathbf{s}_I^{\triangleleft}} + \dots \\ &\quad + \mathbf{b}_{\mathbf{s}_I^{\triangleleft}}^T \mathbf{A}_{\mathbf{s}_{I-1}^{\triangleleft}} \cdots \mathbf{A}_{\mathbf{s}_1^{\triangleleft}} \mathbf{b}_{\mathbf{s}_I^{\triangleleft}} + \dots + \mathbf{b}_{\mathbf{s}_I^{\triangleleft}}^T \mathbf{b}_{\mathbf{s}_I^{\triangleleft}} \\ &= \mathbf{b}_{\mathbf{s}_I^{\triangleleft}}^T \mathbf{b}_{\mathbf{s}_I^{\triangleleft}} + \dots - \mathbf{b}_{\mathbf{s}_I^{\triangleleft}}^T \mathbf{A}_{\mathbf{s}_{I-1}^{\triangleleft}} \cdots \mathbf{A}_{\mathbf{s}_2^{\triangleleft}} \mathbf{b}_{\mathbf{s}_I^{\triangleleft}} + \dots + \mathbf{b}_{\mathbf{s}_I^{\triangleleft}}^T \mathbf{b}_{\mathbf{s}_I^{\triangleleft}} \end{aligned}$$

showing that $\mathbf{c}^T \mathbf{c} = \mathbf{f}^T \mathbf{f}$.

Rewriting the terms $\mathbf{a}^T \mathbf{b}$ and $\mathbf{d}^T \mathbf{e}$ results in

$$\begin{aligned} \mathbf{a}^T \mathbf{b} &= -(\mathbf{p}^{(m)})^T \prod_{i=1}^I \mathbf{A}_{\mathbf{s}_i^{\triangleright}} \mathbf{p}^{(m')} \\ &= -(\mathbf{p}^{(m')})^T \prod_{i=1}^I \mathbf{A}_{\mathbf{s}_{I-i+1}^{\triangleright}}^T \mathbf{p}^{(m)} \\ &= -(\mathbf{p}^{(m')})^T \prod_{i=1}^I \mathbf{A}_{\mathbf{s}_i^{\triangleleft}} \mathbf{p}^{(m)} = \mathbf{d}^T \mathbf{e} \end{aligned}$$

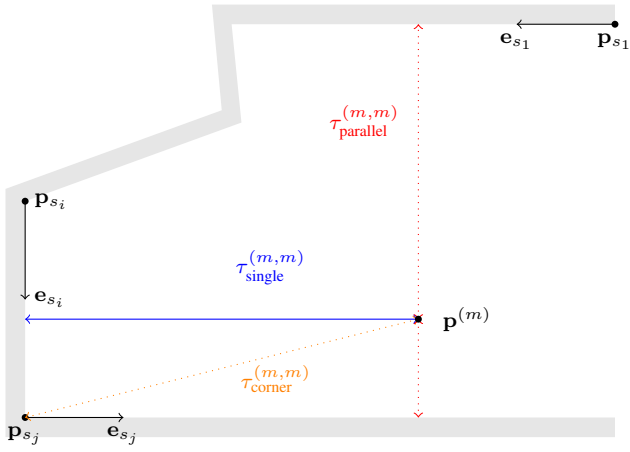


Fig. 9. Illustration of multipath propagation originating from the self-measurement of agent m at position $\mathbf{p}^{(m)}$. The wall segments are described by their location \mathbf{p}_s and direction \mathbf{e}_s . The single-bounce and corner reflection cover information about the agent's position whereas the double-bounce reflection between the parallel walls cannot be exploited for positioning.

applying (22) and the property of symmetry ($\mathbf{A}_{s_i^\triangleright}^\top = \mathbf{A}_{s_i^\triangleleft}$). Finally, $\mathbf{b}^\top \mathbf{c}$ and $\mathbf{d}^\top \mathbf{f}$ follow as

$$\begin{aligned}
\mathbf{b}^\top \mathbf{c} &= (\mathbf{p}^{(m)})^\top \left(\prod_{i=1}^I \mathbf{A}_{s_i^\triangleright} \right)^\top \sum_{i=1}^I \prod_{j=i+1}^I \mathbf{A}_{s_j^\triangleright} \mathbf{b}_{s_j^\triangleright} \\
&= (\mathbf{p}^{(m)})^\top \mathbf{A}_{s_1^\triangleright}^\top \cdots \mathbf{A}_{s_I^\triangleright}^\top \mathbf{A}_{s_I^\triangleright} \mathbf{b}_{s_I^\triangleright} + \dots \\
&\quad + (\mathbf{p}^{(m)})^\top \mathbf{A}_{s_1^\triangleright}^\top \cdots \mathbf{A}_{s_I^\triangleright}^\top \mathbf{b}_{s_I^\triangleright} \\
&= -(\mathbf{p}^{(m)})^\top \mathbf{b}_{s_1^\triangleright} - \dots - (\mathbf{p}^{(m)})^\top \mathbf{A}_{s_1^\triangleright}^\top \cdots \mathbf{A}_{s_{I-1}^\triangleright}^\top \mathbf{b}_{s_I^\triangleright} \\
&= -(\mathbf{p}^{(m)})^\top \mathbf{b}_{s_1^\triangleleft} - \dots - (\mathbf{p}^{(m)})^\top \mathbf{A}_{s_1^\triangleleft}^\top \cdots \mathbf{A}_{s_2^\triangleleft}^\top \mathbf{b}_{s_2^\triangleleft} \\
&= -(\mathbf{p}^{(m)})^\top \sum_{i=1}^I \prod_{j=i+1}^I \mathbf{A}_{s_j^\triangleleft} \mathbf{b}_{s_j^\triangleleft} = \mathbf{d}^\top \mathbf{f} \quad (25)
\end{aligned}$$

and similarly to (25), $\mathbf{a}^\top \mathbf{c} = \mathbf{e}^\top \mathbf{f}$.

APPENDIX C

GRADIENT OF SELF AND RELATIVE MEASUREMENTS

1) *Gradient of self measurements:* Figure 9 illustrates the self-measurement of agent m containing a single-bounce and two double-bounce reflections, one at parallel walls ($\mathbf{s}_{\text{parallel}}^{(m,m)} = [s_1, s_j]$) and one at a corner ($\mathbf{s}_{\text{corner}}^{(m,m)} = [s_i, s_j]$). Due to their regular occurrence in multipath propagation, these reflections are treated in more detail, in the following.

In case of the single-bounce reflection the vector of reflecting segments is $\mathbf{s}_{\text{single}}^{(m,m)} = [s_i]$ and (2) follows as

$$\tau_{\text{single}}^{(m,m)} = \frac{1}{c} d(\mathbf{p}^{(m)}, \mathbf{p}^{(m)}, \mathbf{s}_{\text{single}}^{(m,m)}) = \frac{1}{c} \|2\mathbf{T}_{s_i}(\mathbf{p}^{(m)} - \mathbf{p}_{s_i})\|.$$

The gradient with respect to the agent's position results in

$$\frac{\partial \tau_{\text{single}}^{(m,m)}}{\partial \mathbf{p}^{(m)}} = 2 \underbrace{\frac{2\mathbf{T}_{s_i}(\mathbf{p}^{(m)} - \mathbf{p}_{s_i})}{c \|2\mathbf{T}_{s_i}(\mathbf{p}^{(m)} - \mathbf{p}_{s_i})\|}}_{\boldsymbol{\xi}} \quad (26)$$

where $\boldsymbol{\xi}$ is the normalized direction of the incident multipath, scaled by $1/c$. The scaling factor of 2 indicates that an agent's

position movement $\Delta \mathbf{p}$ towards the wall segment results in a doubled time lag of the MPC along the delay domain.

The gradient with respect to the wall segment location \mathbf{p}_{s_i} follows equivalently to (26) as

$$\frac{\partial \tau_{\text{single}}^{(m,m)}}{\partial \mathbf{p}_{s_i}} = -2\boldsymbol{\xi} = -\frac{\partial \tau_{\text{single}}^{(m,m)}}{\partial \mathbf{p}^{(m)}} \quad (27)$$

and demonstrates that the wall segment location's gradient is in opposite direction to the agent's position gradient.

In case of a double-bounce reflection, two wall segments are involved. If both wall segments are aligned in parallel (e.g. $\{s_1, s_j\}$), then $\mathbf{e}_{s_1} = \pm \mathbf{e}_{s_j}$ and (2) reduces to

$$\tau_{\text{parallel}}^{(m,m)} = \frac{1}{c} \|2\mathbf{T}_{s_1} \mathbf{p}_{s_1} - 2\mathbf{T}_{s_j} \mathbf{p}_{s_j}\|$$

showing that the MPC's delay $\tau_{\text{parallel}}^{(m,m)}$ is independent on the agent's position. Hence, double-bounce reflections originating from parallel walls convey information of wall segments only but cannot be used for positioning of the agents.

Finally, if the affected wall segments are aligned in orthogonal directions (e.g. $\{s_i, s_j\}$) then $\mathbf{e}_{s_i}^\top \mathbf{e}_{s_j} = 0$, $\mathbf{T}_{s_i} + \mathbf{T}_{s_j} = \mathbf{I}$ and the MPC's delay follows as

$$\tau_{\text{corner}}^{(m,m)} = \frac{1}{c} \|2\mathbf{p}^{(m)} - 2\mathbf{T}_{s_i} \mathbf{p}_{s_i} - 2\mathbf{T}_{s_j} \mathbf{p}_{s_j}\|$$

Its derivative with regard to the agent's position is

$$\frac{\partial \tau_{\text{corner}}^{(m,m)}}{\partial \mathbf{p}^{(m)}} = 2 \underbrace{\frac{2\mathbf{p}^{(m)} - 2\mathbf{T}_{s_i} \mathbf{p}_{s_i} - 2\mathbf{T}_{s_j} \mathbf{p}_{s_j}}{c \|2\mathbf{p}^{(m)} - 2\mathbf{T}_{s_i} \mathbf{p}_{s_i} - 2\mathbf{T}_{s_j} \mathbf{p}_{s_j}\|}}_{\boldsymbol{\zeta}}. \quad (28)$$

Similar to a single-bounce reflection (26) an agent's position movement towards the corner results in a doubled time lag of the MPC along the delay domain. The derivative with regard to the wall segment locations is

$$\frac{\partial \tau_{\text{corner}}^{(m,m)}}{\partial \mathbf{p}_{s_i}} = -2\mathbf{T}_{s_i} \boldsymbol{\zeta}, \quad \frac{\partial \tau_{\text{corner}}^{(m,m)}}{\partial \mathbf{p}_{s_j}} = -2\mathbf{T}_{s_j} \boldsymbol{\zeta}$$

showing that the MPC direction $\boldsymbol{\zeta}$ is decomposed in two components, $-2\mathbf{T}_{s_i} \boldsymbol{\zeta}$ and $-2\mathbf{T}_{s_j} \boldsymbol{\zeta}$. The sum of both gradients is equal to the agent's one (but in opposite direction)

$$\frac{\partial \tau_{\text{corner}}^{(m,m)}}{\partial \mathbf{p}_{s_i}} + \frac{\partial \tau_{\text{corner}}^{(m,m)}}{\partial \mathbf{p}_{s_j}} = -\frac{\partial \tau_{\text{corner}}^{(m,m)}}{\partial \mathbf{p}^{(m)}}.$$

In general, these gradients are always perpendicular to the wall segments enforced by matrices $\{\mathbf{T}_s\}$. The angle between the wall segment alignment and the bouncing MPC scales the magnitude of the gradient.

2) *Gradient of relative measurements:* Figure 10 exemplifies delays of deterministic MPCs obtained by a relative measurement between the transmitting agent m' and the receiving agent m consisting of an LOS and two additional reflections. The delay of the LOS $\tau_{\text{LOS}}^{(m',m)}$ is independent of wall segments and (2) follows as

$$\tau_{\text{LOS}}^{(m',m)} = \frac{1}{c} \|\mathbf{p}^{(m)} - \mathbf{p}^{(m')}\|$$

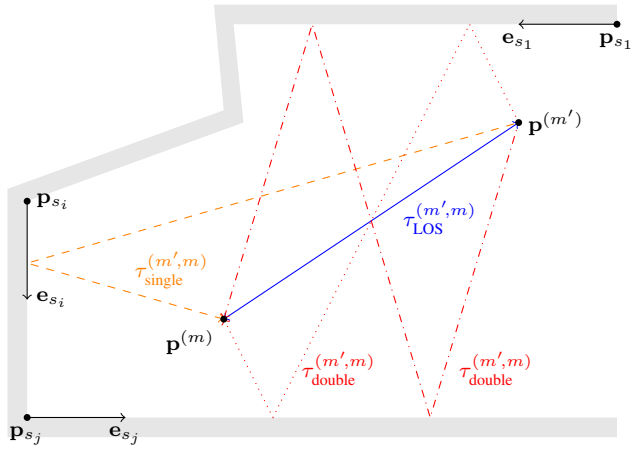


Fig. 10. Illustration of multipath propagation of the relative measurement between the transmitting agent m' and receiving agent m .

Its gradient with respect to both agents results in

$$\begin{aligned} \frac{\partial \tau_{\text{LOS}}^{(m',m)}}{\partial \mathbf{p}^{(m')}} &= \frac{\mathbf{p}^{(m')} - \mathbf{p}^{(m)}}{c \|\mathbf{p}^{(m)} - \mathbf{p}^{(m')}\|} \\ \frac{\partial \tau_{\text{LOS}}^{(m',m)}}{\partial \mathbf{p}^{(m)}} &= \frac{\mathbf{p}^{(m)} - \mathbf{p}^{(m')}}{c \|\mathbf{p}^{(m)} - \mathbf{p}^{(m')}\|} \end{aligned} \quad (29)$$

demonstrating that their gradient is in opposite directions $\partial \tau_{\text{LOS}}^{(m',m)} / \partial \mathbf{p}^{(m')} = -\partial \tau_{\text{LOS}}^{(m',m)} / \partial \mathbf{p}^{(m)}$. The gradient of the MPC delays $\tau_{\text{single}}^{(m',m)}$ and $\tau_{\text{double}}^{(m',m)}$ is obtained similarly to (29) by computing the derivative of (2) with regard to the agents' positions $\mathbf{p}^{(m)}$ and $\mathbf{p}^{(m')}$.

We can conclude that the gradient of agent m depends on the position of the cooperating agent m' . This is in contrast to the self measurements where the delays of the MPCs are independent of other agent positions. Furthermore the obtained delays of the relative measurements are less sensitive to agents' position movements compared to the self measurements (due to a missing factor of 2 which arises at (27) or (28)).

REFERENCES

- [1] H. Wymeersch, J. Lien, and M. Z. Win, "Cooperative localization in wireless networks," *Proceedings of the IEEE*, 2009.
- [2] L. Cong and W. Zhuang, "Non-line-of-sight error mitigation in mobile location," in *INFOCOM 2004. Twenty-third Annual Joint Conference of the IEEE Computer and Communications Societies*, vol. 1, March 2004.
- [3] S. Marano, W. M. Gifford, H. Wymeersch, and M. Z. Win, "NLOS identification and mitigation for localization based on UWB experimental data," *IEEE Journal on Selected Areas in Communications*, vol. 28, no. 7, pp. 1026–1035, 2010.
- [4] H. Wymeersch, S. Marano, W. Gifford, and M. Win, "A machine learning approach to ranging error mitigation for UWB localization," *IEEE Transactions on Communications*, 2012.
- [5] A. Conti, D. Dardari, M. Guerra, L. Mucchi, and M. Win, "Experimental characterization of diversity navigation," *IEEE Systems Journal*, 2014.
- [6] Y. Shen, S. Mazuelas, and M. Win, "Network navigation: theory and interpretation," *IEEE Journal on Selected Areas in Communications*, 2012.
- [7] E. Leitinger, P. Meissner, C. Ruedisser, G. Dumphart, and K. Witrisal, "Evaluation of position-related information in multipath components for indoor positioning," *IEEE Journal on Selected Areas in Communications*, 2015.
- [8] E. Tsalolikhin, I. Bilik, and N. Blaunstein, "A single-base-station localization approach using a statistical model of the NLOS propagation conditions in urban terrain," *IEEE Transactions on Vehicular Technology*, vol. 60, no. 3, 2011.
- [9] K. Witrisal, P. Meissner, E. Leitinger, Y. Shen, C. Gustafson, F. Tufvesson, K. Haneda, D. Dardari, A. F. Molisch, A. Conti, and M. Z. Win, "High-accuracy localization for assisted living," *IEEE Signal Processing Magazine*, 2016.
- [10] R. Parhizkar, I. Dokmanic, and M. Vetterli, "Single-channel indoor microphone localization," in *2014 IEEE International Conference on Acoustics, Speech and Signal Processing (ICASSP)*, May 2014.
- [11] S. V. de Velde and H. Steendam, "CUPID algorithm for cooperative indoor multipath-aided localization," in *2012 International Conference on Indoor Positioning and Indoor Navigation (IPIN)*, Nov 2012.
- [12] S. Van de Velde, H. Wymeersch, P. Meissner, K. Witrisal, and H. Steendam, "Cooperative multipath-aided indoor localization," in *2012 IEEE Wireless Communications and Networking Conference (WCNC)*. IEEE, 2012.
- [13] H. Naseri, M. Costa, and V. Koivunen, "Multipath-aided cooperative network localization using convex optimization," in *2014 48th Asilomar Conference on Signals, Systems and Computers*, Nov 2014.
- [14] M. Froehle, E. Leitinger, P. Meissner, and K. Witrisal, "Cooperative multipath-Assisted Indoor Navigation and Tracking (Co-MINT) Using UWB Signals," in *IEEE ICC Workshop on Advances in Network Localization and Navigation*, 2013.
- [15] J. Kulmer, E. Leitinger, P. Meissner, and K. Witrisal, "Cooperative Multipath-assisted Navigation and Tracking: A Low-Complexity Approach," in *1st EAI International Conference on Future access enablers of ubiquitous and intelligent infrastructures*, 2015. EAI, 2015.
- [16] J. Kulmer, E. Leitinger, P. Meissner, S. Hinteregger, and K. Witrisal, "Cooperative localization and tracking using multipath channel information," in *2016 International Conference on Localization and GNSS (ICL-GNSS)*, June 2016.
- [17] H. Miao, K. Yu, and M. J. Juntti, "Positioning for NLOS propagation: algorithm derivations and Cramer Rao bounds," *IEEE Transactions on Vehicular Technology*, vol. 56, no. 5, pp. 2568–2580, Sept 2007.
- [18] W. Xu, F. Quitin, M. Leng, W. P. Tay, and S. G. Razul, "Distributed localization of a RF target in NLOS environments," *IEEE Journal on Selected Areas in Communications*, vol. 33, no. 7, July 2015.
- [19] S. Thrun, W. Burgard, and D. Fox, *Probabilistic Robotics*. MIT, 2005.
- [20] C. Gentner, T. Jost, W. Wang, S. Zhang, A. Dammann, and U. C. Fiebig, "Multipath assisted positioning with simultaneous localization and mapping," *IEEE Transactions on Wireless Communications*, no. 99, 2016.
- [21] C. Gentner, B. Ma, M. Ulmschneider, T. Jost, and A. Dammann, "Simultaneous localization and mapping in multipath environments," in *2016 IEEE/ION Position, Location and Navigation Symposium (PLANS)*, April 2016, pp. 807–815.
- [22] P. Setlur, T. Negishi, N. Devroye, and D. Erricolo, "Multipath exploitation in non-LOS urban synthetic aperture radar," *IEEE Journal of Selected Topics in Signal Processing*, vol. 8, no. 1, pp. 137–152, Feb 2014.
- [23] Y. Shen and M. Win, "Fundamental limits of wideband localization; part I: a general framework," *IEEE Transactions on Information Theory*, 2010.
- [24] Y. Shen, H. Wymeersch, and M. Win, "Fundamental limits of wideband localization - part II: cooperative networks," *IEEE Transactions on Information Theory*, 2010.
- [25] M. Z. Win, A. Conti, S. Mazuelas, Y. Shen, W. M. Gifford, D. Dardari, and M. Chiani, "Network localization and navigation via cooperation," *IEEE Communications Magazine*, vol. 49, no. 5, pp. 56–62, May 2011.
- [26] K. Witrisal and P. Meissner, "Performance bounds for multipath-assisted indoor navigation and tracking (MINT)," in *IEEE International Conference on Communications (ICC)*, 2012.
- [27] A. Molisch, "Ultra-wide-band propagation channels," *Proceedings of the IEEE*, 2009.
- [28] C. Falsi, D. Dardari, L. Mucchi, and M. Z. Win, "Time of arrival estimation for UWB localizers in realistic environments," *EURASIP Journal on Advances in Signal Processing*, vol. 2006, no. 1, 2006.
- [29] P. Meissner, E. Leitinger, and K. Witrisal, "UWB for robust indoor tracking: weighting of multipath components for efficient estimation," *IEEE Wireless Communications Letters*, vol. 3, no. 5, pp. 501–504, Oct. 2014.
- [30] A. Molisch, *Wireless Communications*. Wiley, 2007.
- [31] J. Munkres, "Algorithms for the assignment and transportation problems," *Journal of the Society for Industrial and Applied Mathematics*, vol. 5, no. 1, pp. 32–38, 1957.

- [32] D. Schuhmacher, B.-T. Vo, and B.-N. Vo, "A consistent metric for performance evaluation of multi-object filters," *IEEE Transactions on Signal Processing*, 2008.
- [33] Ilmsens Channel Sounder. [Online]. Available: <http://www.ilmsens.com>
- [34] P. Meissner, E. Leitinger, M. Lafer, and K. Witrisal, "MeasureMINT UWB database," 2013, Publicly available database of UWB indoor channel measurements.
- [35] C. Krall, "Signal processing for ultra wideband transceivers," Ph.D. dissertation, Graz University of Technology, Austria, 2008.
- [36] H. Schantz, "Planar elliptical element ultra-wideband dipole antennas," in *IEEE Antennas and Propagation Society International Symposium*, vol. 3. IEEE; 1999, 2002, pp. 44–47.
- [37] Mini Circuits, RC-4SPDT-A18 and RC-ISP4T-A18. [Online]. Available: <http://www.minicircuits.com>
- [38] P. Meissner and K. Witrisal, "Multipath-Assisted Single-Anchor Indoor Localization in an Office Environment," in *19th International Conference on Systems, Signals and Image Processing (IWSSIP)*, Vienna, Austria, 2012, invited paper.
- [39] B. Eitzlinger, H. Wymeersch, and A. Springer, "Cooperative synchronization in wireless networks," *IEEE Trans. Signal Processing*, vol. 62, no. 11, pp. 2837–2849, 2014.
- [40] J. Kulmer, S. Hinteregger, B. Großwindhager, M. Rath, M. Bakr, E. Leitinger, and K. Witrisal, "Using DecaWave UWB Transceivers for High-accuracy Multipath-assisted Indoor Positioning," in *IEEE ICC 2017 Workshop on Advances in Network Localization and Navigation (ANLN)*, 2017.
- [41] J. Borish, "Extension of the image model to arbitrary polyhedra," *The Journal of the Acoustical Society of America*, vol. 75, no. 6, 1984.